ACS NANO
Cite This: ACS Nano 2018, 12, 1179–1187
www.acsnano.org
ARTICLE

Electric-Field-Guided Precision Manipulation of Catalytic Nanomotors for Cargo Delivery and Powering Nanoelectromechanical Devices

Jianhe Guo,[†] Jeremie June Gallegos,[‡] Ashley Robyn Tom,[‡] and Donglei Fan*[,†,‡]

[†]Materials Science and Engineering Program and [‡]Department of Mechanical Engineering, The University of Texas at Austin, Austin, Texas 78712, United States

Supporting Information

ABSTRACT: We report a controllable and precision approach in manipulating catalytic nanomotors by strategically applied electric (*E*-) fields in three dimensions (3-D). With the high controllability, the catalytic nanomotors have demonstrated versatility in capturing, delivering, and releasing of cargos to designated locations as well as *in situ* integration with nanomechanical devices (NEMS) to chemically power the actuation. With combined AC and DC *E*-fields, catalytic nanomotors can be accurately aligned by the AC *E*-fields and effectively change their speeds instantly by the DC *E*-fields. Within the 3-D orthogonal microelectrode sets, the in-plane transport of catalytic nanomotors can be swiftly turned on and off, and these catalytic nanomotors can also move in the vertical direction. The interplaying nanoforces that govern the propulsion and alignment are investigated. The modeling of catalytic nanomotors proposed in previous works has been confirmed quantitatively here. Finally, the prowess of the precision manipulation of catalytic nanomotors by *E*-fields is demonstrated in two applications: the capture, transport, and release of cargos to prepatterned microdocks, and the assembly of catalytic nanomotors on NEMS to power the continuous rotation. The concepts and approaches reported in this work could further advance applications of catalytic nanomotors, *e.g.*, for assembling and powering nanomachines, nanorobots, and complex NEMS devices.

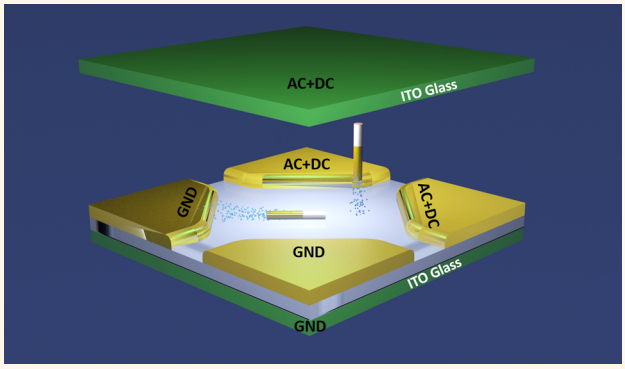

KEYWORDS: *nanomotors, catalytic nanomotors, electric tweezers, cargo delivery, NEMS, rotary NEMS, nanorobotics*

The integration of autonomous inorganic micro-/nanomotors as components of micro-/nanomachines with high precision and versatility to power their operations is a critical step in realizing the applications in nanofactories and nanorobots, which could revolutionize modern lives.[1−10] In the past decade, the development of micro-/nanomotors has advanced rapidly since the early stages of exploration.[11−14] Nanomotors can propel themselves by harnessing energy either from chemical reactions in the environment or from external physical fields. The precision control of the position and strength of external physical fields (including optical,[15,16] magnetic,[17−21] electrical fields,[22−25] and ultrasonic waves)[26−28] lead to a variety of manipulation approaches for cargo transport, drug delivery, biochemical sensing, and cell trapping. Catalytic micro-/nanomotors represent another important class of autonomous nanomotors that convert chemical energy into mechanical motions, mimicking biomolecular motors in nature.[13,29−36] Billions of catalytic nanomotors can be facilely fabricated by using a variety of techniques, such as electrodeposition into nanoporous templates and electron beam deposition on monolayer nanospheres.[1,2] They self-propel by harvesting chemical energies from fuels in suspension, such as hydrogen peroxide.[13,37] Recently, substantial research efforts have been focused on strategically designing and fabricating catalytic nanomotors with an array of compositions and geometries, such as bimetallic nanorods,[13,37,38] catalytic microtubes,[39−41] and Janus particles.[42−45] The efforts lead toward dramatic improvement of propulsion speeds up to hundreds of μm/s (or 100 body lengths per second)[37−39] and readiness in harnessing energy from a variety of fuels, such as hydrazine,[46] urea,[47,48] and even pure water.[32,44,49] More importantly, vast applications of catalytic nanomotors have been demonstrated, such as on-chip cargo transport,[42,50] drug delivery,[51,52] microchip repair,[53]

Received: September 25, 2017
Accepted: January 5, 2018
Published: January 5, 2018

DOI: 10.1021/acsnano.7b06824
ACS Nano 2018, 12, 1179–1187

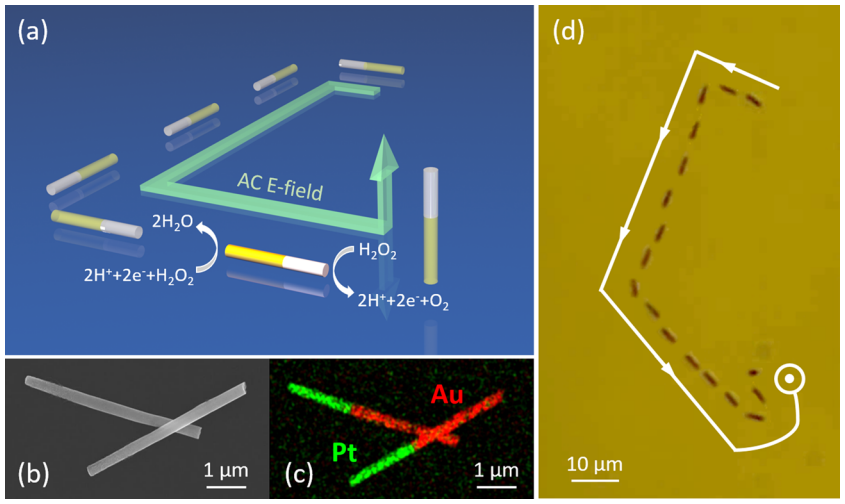

Figure 1. (a) Schematic diagram of 3D manipulations of Pt−Au catalytic nanomotors in H_2O_2 fuel with AC *E*-fields. (b) Scanning electron microscopy (SEM) and (c) energy-dispersive X-ray spectroscopy (EDX) images of Pt−Au catalytic nanomotors (250 nm in diameter, 5 μm in length; consisting of 2 μm Pt segment and 3 μm Au segment). (d) Overlapped snapshots of a catalytic nanomotor guided by AC *E*-fields.

nanolithography,[54] biomolecular sensing, and *in vivo* disease treatment.[55]

However, it remains challenging to align catalytic nanomotors with high precision and modulate their moving speeds facilely and instantly. Innovatively, magnetic fields have been exploited in guiding catalytic nanomotors; however, this strategy requires the integration of magnetic elements in the nanomotors and precise alignment of magnetic moments.[42,50] Also, to generate magnetic forces, bulky electromagnets are often employed, which could be the bottleneck when developing portable nanomotor based devices. Acoustic tweezers have been used in guiding catalytic nanomotors to aggregate and disperse,[56] while the resolution in manipulation is restricted by the large wavelength of acoustic waves. Besides controlling the orientation of catalytic nanomotors, it is of paramount importance to facilely tune their speed. Several unique approaches have been exploited to control locomotion speed of catalytic nanomotors. With the strong dependence on catalytic reactivity, the speed of catalytic micro-/nanomotors can be tuned by localized stimuli, including fuel concentration,[13] temperature,[57] and light illumination.[44,58−60] Furthermore, by applying electrical potentials to create chemical gradient,[61] or generating ultrasonic waves,[56,62] the speed of micro-/nanomotors can also be modulated. However, it remains difficult to realize both the guiding and speed tuning of catalytic nanomotors with high accuracy, facileness, and in an all-on-chip manner.

In this work, we report a versatile approach for manipulating catalytic nanomotors with high precision and facileness. The work is based on strategically combined AC and DC *E*-fields, the so-called electric tweezers, applied *via* a 3-D orthogonal microelectrode setup.[63] Here, the DC *E*-field tunes the transport speed *via* electrophoretic and electroosmosis effects. The AC *E*-field guides the alignment independently *via* electric torques on the induced dipoles of nanomotors. By applying the combined AC and DC *E*-fields in 3-D, catalytic nanomotors can instantly align, transport along defined directions, start and stop, and change speeds on demand. The involved various nanoforces governing the motions are investigated. Leveraging the high precision in the alignment, the linear dependence of speed on the inverse of size of nanomotors ($1/l$) down to submicrometers, is experimentally determined, confirming previous theoretical predictions.[33] Finally, the manipulation of catalytic nanomotors by *E*-fields is demonstrated for two applications: the dynamic loading, transport, and unloading of microtargets to prepatterned microdocks; and assembling and integration of a catalytic nanomotor on a rotary NEMS to power its continuous operation.

RESULTS AND DISCUSSION

Guide, Start and Stop, and Modulate Speed of Catalytic Nanomotors. The demonstrations of transport guidance and speed modulation of catalytic nanomotors by *E*-fields are carried out by using the classical Pt-based bimetallic nanorod motors as a model system (Figure 1a). Arrays of multisegmented Pt−Au nanorod motors are synthesized with controlled lengths and diameters by electrodeposition into nanoporous templates in a three-electrode setup.[13,64] The fabrication details are provided in the Methods. Scanning electron microscopy (SEM) and energy-dispersive X-ray spectroscopy (EDS) in Figure 1b,c confirm the uniform cylindrical morphology, controlled size, and composition of the Pt−Au catalytic nanomotors.

A software interfaced 3-D orthogonal microelectrode setup is designed and constructed for guiding the catalytic nanomotors as shown in Figure 2. By applying an AC *E*-field on the in-plane quadruple microelectrodes, the catalytic nanomotors can be instantly aligned along the direction of the AC *E*-field and move

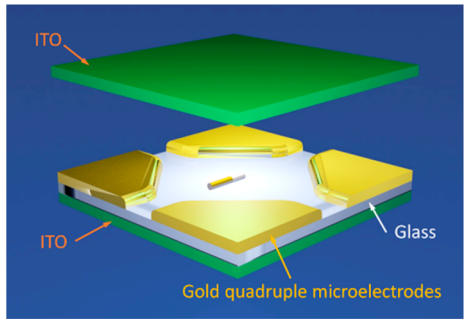

Figure 2. Scheme of 3-D orthogonal microelectrode setup.

DOI: 10.1021/acsnano.7b06824
ACS Nano 2018, 12, 1179−1187

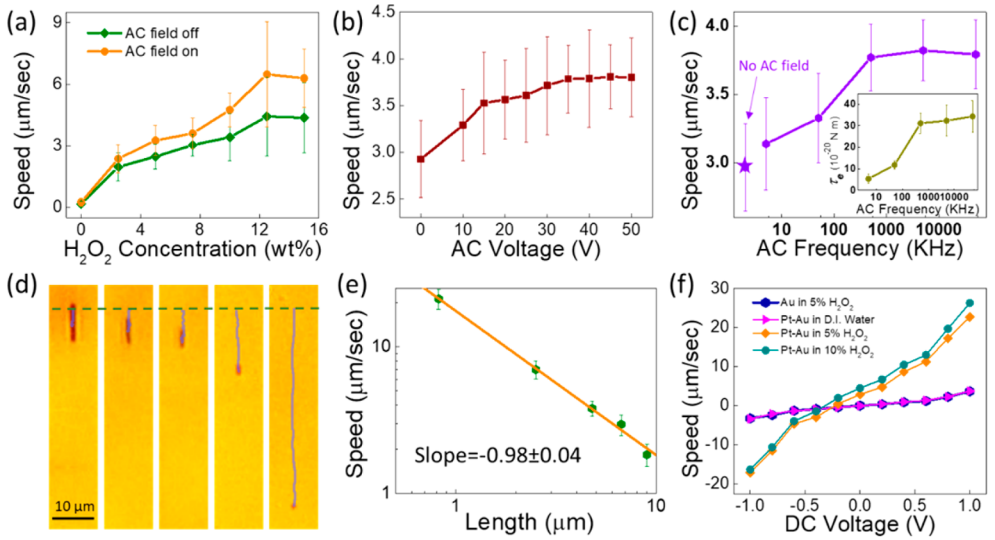

Figure 3. (a) Speed of catalytic nanomotors *versus* concentration of H_2O_2 with/without AC *E*-fields (5 MHz, 15 V). (b) Speed *versus* peak-to-peak voltage of AC *E*-fields (500 kHz) in 7.5 wt % H_2O_2 solution. (c) Speed *versus* frequency of AC *E*-fields (20 V) in 7.5 wt % H_2O_2 solution. Inset: electric torque *versus* frequency of AC *E*-fields. (d) Trace of catalytic nanomotors of different lengths in 7.5 wt % H_2O_2 solution with AC *E*-fields (5 MHz, 15 V) in 2 s. The lengths of nanomotors (from right to left) are 0.82, 2.50, 4.78, 6.68, and 8.96 μm, respectively. The green dashed line shows the starting position. (e) Log−log plot of speed *versus* length of nanomotors in (d). The slope is −0.98. (f) Speed of Au nanorods and Pt−Au catalytic nanomotors of same dimensions *versus* DC *E*-fields in different suspension mediums.

autonomously in the direction with the Pt segment as the front, as shown in the schematic diagram in Figure 1a, overlapped images in Figure 1d, and movie S1. We found that an AC peak-to-peak voltage of 10 V is sufficient to align the catalytic nanomotors and to guide their motions. When superimposing a DC *E*-field on the AC *E*-field, the speed of the nanomotors can increase or decrease instantaneously, and even reverse the moving direction. We characterize the manipulation in detail in the following to unveil the fundamental interactions between the nanomotors and *E*-fields.

First, we investigate the dependence of speed of the catalytic nanomotors on the concentration of hydrogen peroxide fuel (H_2O_2), both with and without *E*-fields. The average speed of the catalytic nanomotors is determined statistically from the behaviors of 10 nanomotors for 10 s (details in the Supporting Information). As shown in Figure 3a, regardless whether the *E*-field is applied or not, the speed of the nanomotors increases with the concentration of H_2O_2 and reaches a plateau, which can be attributed to the saturation of catalytic active sites on the nanomotors in high concentration H_2O_2 fuels.[13] Consistently, we find that the speed of these catalytic nanomotors under AC *E*-fields is always higher than those without AC *E*-fields. Furthermore, the speed of all nanomotors, regardless of their moving directions, increases when applying a uniform AC *E*-field. Neither the electroosmosis flows nor the induced dielectrophoretic forces could result in the observed behavior, so the dominating factor is the reduction of rotational Brownian motions of nanomotors due to the alignment by AC *E*-fields. Our experimental results and analysis support this understanding. First, we determine the speed of nanomotors as a function of AC frequency and voltage. It is found that the average speed of nanomotors monotonically increases with AC frequency before reaching a constant at around 500 kHz and 20 V (peak to peak, same for the following AC voltages). At a fixed AC frequency, *i.e.*, 500 kHz, the average speed also increases with AC voltage amplitude until a constant is reached at 30 V as shown in Figure 3b,c. The voltage dependence can be readily understood from the increase of electric torque (τ_e) with applied *E*-field (E), which counters the rotational Brownian motions and thus enhances the degree of alignment of a nanomotor, given by[65]

$$\tau_e = \frac{8\pi l r^2}{3} P E^2 \sin 2\theta \quad (1)$$

where l and r are the length and radius of nanomotor, respectively; θ is the angle between the long axis of nanomotor and the *E*-field; and P is a value determined by the permittivity and conductivity of the medium and nanomotor as well as the AC frequency. We observe a leveling off of the moving speed when the voltage is adequately high, *i.e.*, above 30 V, as shown in Figure 3b. It could be understood that when the electric torque is sufficiently high, the rotational Brownian motion is suppressed to an extent that the increase of speed with voltages is too small to be determined compared to the statistic distributions of speed of tested nanomotors.

By analyzing electric torques, we can also attribute the observed dependence of nanomotor speed on AC frequency (Figure 3c) to the suppressed rotational Brownian motions. We experimentally determine electric torques as a function of angular positions when aligning nanomotors at 5 kHz to 50 MHz with eq 1. The τ_e exerted on the catalytic nanomotors at an angle of θ can be readily obtained from the angular velocity (ω) *versus* angle (θ) (Figure S1), since the viscous torque (τ_η) instantly counters the electric torque (τ_e) as given by $\tau_e = \tau_\eta$ in low Reynolds number environment. Here, the viscous drag torque τ_η on a rotating nanorod is calculated as follows[22]

$$\tau_\eta = \frac{1}{3}\omega\pi\eta l^3 \frac{N^3 - N}{N^3\left(\ln\frac{l}{Nr} + 0.5\right)} = K_1\omega(Nm) \quad (2)$$

where η is the viscous coefficient of suspension medium and N is the number of nanorod segments, taken as 2 in this calculation. For the nanomotors used in our experiments, the constant K_1 is determined as 2.50×10^{-20}. Now, with τ_e

DOI: 10.1021/acsnano.7b06824
ACS Nano 2018, 12, 1179−1187

determined at different θ from eq 1 and (2), we can readily obtain the coefficient of τ_e at different AC frequencies as shown in Figure 3c. It can be readily found that the dependence of nanomotor speed on AC frequency well matches the dependence of electric torque applied on nanomotors *versus* AC frequency. It well supports the key contribution of alignment by AC *E*-fields to the observed enhanced speed of nanomotors.

With the uniform AC *E*-fields, we not only improve the alignment and speed of nanomotors as discussed as above, but also successfully guided catalytic nanomotors in the vertical direction in a facile and all-on-chip manner. Nanomotors can move along prescribed trajectories in the 2-D $X-Y$ plane, start and stop on demand, and even move vertically as shown in Figure 1a and movies S1 and S2. For nanomotors moving in the $X-Y$ 2-D plane, it is known that the catalytic driving force balances with the drag force, given by[22]

$$F_{\text{catalytic drive}} = F_{\text{drag}} = \frac{2\pi\eta l}{\ln\frac{l}{r} - 0.5}\nu = K_2\nu(N) \tag{3}$$

where ν is the velocity of catalytic nanomotors and the geometric factor $K_2 = 8.77 \times 10^{-9}$ for the tested nanomotors (5 μm in length and 250 nm in diameter). Note that the value of viscous coefficient η of suspension medium is estimated from that of pure water at room temperature, knowing that the change of viscous coefficient is less than 3% when the concentration of H_2O_2 is less than 10 wt %.[66] In the vertical direction, a catalytic nanorod made of Pt(2-μm)-Au(3-μm) experiences gravitational and buoyant forces of $4.85 \times 10^{-14}N$ and $0.24 \times 10^{-14}N$, respectively. Therefore, from eq 3 and the experimental results of velocity *versus* fuel concentration (C_{H2O2}) shown in Figure 3a, we can readily determine that the catalytic driving force of nanomotors is sufficiently high to realize the propulsion of the nanomotor in the vertical direction when the concentration of fuel (C_{H2O2}) is above 10 wt %. This analysis is validated by experimental study as shown in move S2. When C_{H2O2} is 12.5 wt %, where a driving force of $5.69 \times 10^{-14}N$ is determined by calculation, the catalytic nanomotors indeed aligned and transported vertically, overcoming gravitation forces, and gradually disappeared from the view. While at a lower fuel concentration, *e.g.*, when C_{H2O2} is 7.5 wt %, a vertically applied AC *E*-field can instantly align nanomotors vertically and stop the motions in 2-D planes. Here the driving forces due to catalytic reactions, calculated as $3.17 \times 10^{-14}N$, is not sufficient to propel the motors vertically. Both the demonstrations of 3-D manipulation at high fuel concentrations and "on/off" control of 2-D motion at low fuel concentrations offer considerable promise for versatile operations of these catalytic nanomotors, opening many opportunities for applications. Such a strategy could also be applied for controlling photocatalytic nanomotors[44,59] and self-propelled enzyme nanomotors.[31,48]

The high precision in the alignment of nanomotors by AC *E*-fields offers opportunities in studying and understanding the working mechanism of the self-propelled catalytic nanomotors. The dominant propulsion mechanism of catalytic nanomotors is suggested as self-electrophoresis based on the electrocatalytic decomposition of hydrogen peroxide.[67,68] In a recent model of a catalytic nanomotor made of bimetallic nanorods, the velocity (ν) due to self-electrophoresis is given by[33]

$$\nu \sim \frac{\zeta_p\varepsilon\varepsilon_0}{\eta}E_{\text{int}} \sim \frac{\zeta_p\varepsilon\varepsilon_0\Delta\phi}{\eta l} \tag{4}$$

where ε is the relative dielectric constant of the suspension medium and ε_0 is the dielectric permittivity of free space. The self-generated *E*-field E_{int} is approximated as the potential drop $\Delta\phi$ divided by the length of the nanorods l and $\Delta\phi$ is determined by the chemical potential of the two metal segments of a nanomotor, which is considered as a constant with different lengths; ζ_p is Zeta potential of a nanomotor, independent of the size of the nanomotor (Figure S4). Therefore, we can readily find that the self-electrophoretic velocity (ν) of a nanomotor should be inversely proportional to its length (l) according to eq 4 as suggested by this model. Although in previous studies it has been shown that the smaller the catalytic nanomotors the higher the moving speed, quantitative study has yet been carried out on the catalytic nanomotors as predicted by the model.[33,69] To experimentally determine the dependence of speed on size of nanomotors, the key is to precisely align nanomotors with controlled moving trajectories and to suppress noises due to Brownian motion. As shown in the above studies, AC *E*-field alignment provides a facile and effective tool, where the alignment is determined by the overall shape anisotropy of a nanomotor. Indeed, with AC *E*-fields, we can synchronously align catalytic nanomotors with sizes ranging from 0.82 to 8.96 μm (details in Figure S5). These nanomotors with different sizes are designed with an identical length ratio of Pt:Au (~2:3). When suspending in H_2O_2 solutions, the shorter nanomotors exhibit higher moving speeds compared to longer ones (Figure 3d). The speed and length of nanomotors follows an inverse proportional relationship as shown in the log–log plot with a slope of -0.98 ± 0.04 in Figure 3e. It indicates that the power law dependence of speed on size of nanomotors is approximately -1, which provides quantitative proof of the working mechanism proposed previously for nanomotors in the size range of 0.82 to 8.96 μm. This result points toward the great advantages of catalytic nanomotors in achieving ultrahigh propulsion speed when made into ultrasmall dimensions.[41,70,71] The involved nanoforces, energy conversion efficiency, and influencing factors, such as impurities, of the catalytic nanomotors have been well studied.[33,67,68,72] For instance, the velocity of nanomotors is inversely proportional to the electric conductivity of the suspension. Given the feasibility of the self-electrophoresis model, we expect the same ionic effect for the catalytic nanomotors guided by the *E*-fields. We notice that the increased conductivity due the present of salt also reduces the electric torque for alignment of nanomotors as shown in the Supporting Information. Therefore, in some biological suspension media with high ionic concentrations and electric conductivities, *e.g.*, cell culture media and cell washing media such as phosphate buffered saline, the catalytic nanomotors have decreased (or even diminished) velocity and weakened electric alignment. It is critical to explore the use of alternative biological media with low electric conductivities. For instance, as we demonstrated previously, in sucrose based biological media, nanowires have been manipulated effectively in both propulsion and alignment by the applied combined AC and DC *E*-fields, which is compatible with live cell experimentation.[23]

Next, we exploit the effect of DC *E*-fields on nanomotors. The speed of the Pt–Au catalytic nanomotors due to DC *E*-fields are tested in pure water and 5–10 wt % H_2O_2 fuels. Gold (Au) nanorods of the same dimension are fabricated and tested

DOI: 10.1021/acsnano.7b06824
ACS Nano 2018, 12, 1179–1187

at the same conditions for control experiments. AC *E*-fields are superimposed to align the nanomotors in their long axis direction when applying DC voltages of −1 to +1 V on 500 μm-gapped microelectrodes. The speed of catalytic nanomotors linearly depends on DC *E*-fields and can be controlled to instantly increase, decrease and even reverse directions, depending on the magnitude and direction of DC *E*-fields as shown in Figure 3f and movie S3. A DC voltage as low as 1 V can lead to a velocity change of ~20 μm/sec of the catalytic nanomotors, which is effective in modulating speed of nanomotors for various applications (Figure 3f).

We also observe that the speeds of both catalytic nanomotors in fuel solutions and those in control experiments always increase in the direction of DC *E*-fields. While the zeta potentials of both Pt−Au nanomotors and Au nanorods are negative as shown in the measurements in Figure S3. Furthermore, although the speed of the catalytic nanomotors show much stronger responses to the DC *E*-field, the value of their zeta potential in fuel solutions is significantly lower than those of control samples, *i.e.*, for Pt−Au nanomotors in 5% H_2O_2 fuel, the zeta potential of −8.76 mV is around 1/4 of those of control samples.

The above phenomena cannot be explained simply by electrophoresis (EP). Nanoentities, such as nanomotors, experience an electrophoretic force in the presence of an external DC *E*-field due to the formation of an electric double layer at the solid/liquid interface with opposite local charges. The speed of nanoentities (ν_{EP}) due to electrophoretic force is proportional to the dielectric constant of suspension medium (ε), zeta potential of nanomotor (ζ), and DC *E*-field (E_{ext}), given by[73]

$$v_{EP} = \frac{\varepsilon\varepsilon_0\zeta}{\eta}\mathbf{E}_{ext} \tag{5}$$

Given that the zeta potentials of the catalytic nanomotors and control samples are all negative, if only because of the electrophoretic effect, the moving speed should increase in the opposite direction of the DC *E*-field and scale with the magnitude of the zeta potential. However, the experiments show the behaviors of nanomotors opposite to this analysis. In-depth study shows that in addition to electrophoretic (EO) forces, electroosmosis flows generated on the surface of glass substrates are important as well, which is given by[73]

$$\mathbf{v}_{EO} = -\frac{\varepsilon\varepsilon_0\zeta_s}{\eta}\mathbf{E}_{ext} \tag{6}$$

The zeta potential of glass substrates (ζ_s) is negative and can reach −80 mV.[74] As a result, the direction of electroosmosis flow on glass substrates is in the same direction of DC *E*-field according to eq 6, opposite to that of the electrophoretic effect on nanomotors in eq 5. Therefore, the speed of a nanomotor (ν_E) in DC *E*-field is governed by the combined effects of electrophoretic force on the nanomotor (ν_{EP}) in eq 5 and electroosmosis flows on the glass substrate (ν_{EO}) in eq 6. Considering the zeta potentials and the moving direction of nanomotors, it can be found that the electroosmosis flows (ν_{EO}) dominate the motions of nanomotors. These results and conclusions are consistent with the reported electroosmosis-based micropumps, where the *E*-fields are generated by catalytic reactions on different materials.[67,75,76] Therefore, lower absolute values of the negative zeta potential of the nanomotors lead to higher speed modulations by the DC *E*-field. This well agrees with the experimental results in Figure 3f, where the speed of catalytic nanomotors can be strongly tuned by the external DC *E*-field (Supporting Information).

With the demonstration and understanding of the prowess of AC and DC *E*-fields for manipulation of catalytic nanomotors with high facileness, precision, and efficiency, we exploited two applications of these catalytic nanomotors: targeted cargo delivery and assembling of catalytic nanomotors for powering rotary NEMS devices.

Targeted Cargo Delivery. In this demonstration (Figure 4a and movie S4), Au nanorods (250 nm in diameter and 3.6 μm in length), fabricated by electrodeposition into nanoporous templates, serve as cargos. They are mixed with Pt−Au catalytic nanomotors in 7.5 wt % H_2O_2 fuel solution. Without AC *E*-field, the catalytic nanomotors move randomly, while the Au cargos only exhibit weak Brownian motions. By applying a uniform AC *E*-field, both nanomotors and cargo nanorods are aligned. The nanomotors move in the alignment direction. While, the cargo stays essentially at the original location during the transport of the nanomotor guided by the AC *E*-field as shown in Figure 4b,c. When the nanomotor are close to the cargo, the induced *E*-fields can readily assemble them tip to tip. Here, the interaction between the induced dipoles of nanomotor and cargo ensures a simple procedure to upload the cargo on the nanomotor and the assembly is robust during the transport in AC *E*-fields. Next, guided by the AC *E*-field, the nanomotor propels the cargo to a patterned metallic microdock as shown in Figure 4c,d. When the cargo is in the vicinity of the microdock, it can rapidly anchor to the edge of the metallic microdock due to the interaction between induced electric dipoles. Then the nanomotor can start its next journey to seek

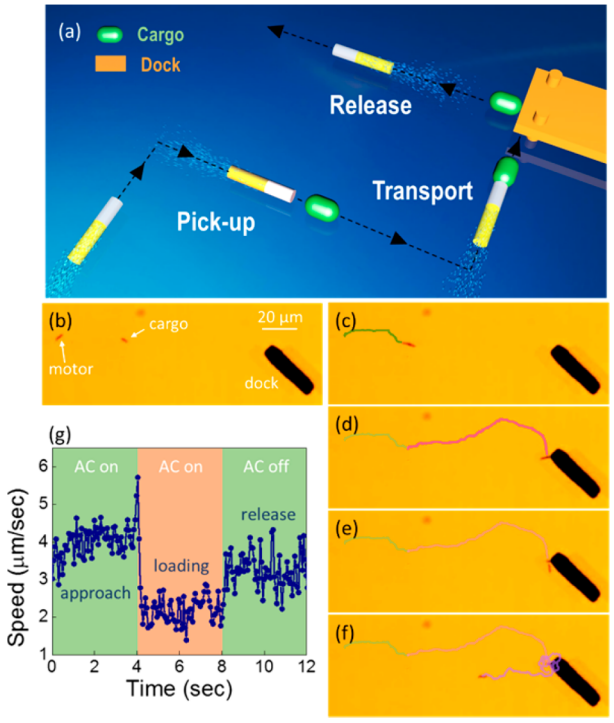

Figure 4. (a) Scheme of targeted cargo delivery. (b−f) Optical microscopy images show the dynamic process of a Pt−Au catalytic nanomotor when picking up, pushing, and delivering a nanorod cargo to the designated microdock. (g) Speed of the nanomotor in the cargo delivery process.

DOI: 10.1021/acsnano.7b06824
ACS Nano 2018, 12, 1179−1187

other targets as shown in Figure 4e,f. Here, the on-demand release of cargos from the catalytic nanomotors are facilely accomplished by turning off the AC *E*-field swiftly, *e.g.*, for a few seconds (Figure 4e). The above process is further determined quantitatively by analyzing the instantaneous speed of nanomotors as shown in Figure 4g. When the nanomotor moves toward the cargo, the average speed is around 3.9 μm/sec. The speed swiftly increases to 5.7 μm/s when it gets close and attaches to the cargo due to the strong mutual attraction. After capturing the cargo, the speed decreases to 2.2 μm/s due to the load, which agrees with our estimation of 2.6 μm/s from eq 3. After releasing the cargo, the nanomotor immediately restores to a speed up to 3.3 μm/s, which is slightly lower than the speed of 3.6 μm/s before loading the cargo. Note that at this moment the nanomotor is not aligned by the AC *E*-field which could account for the lowered speed. The above demonstration of targeted cargo delivery by nanomotors under the control of *E*-field shows simplicity and reliability for diverse lab-on-a-chip applications.

Powering Rotary NEMS by Precision Assembling Catalytic Nanomotors. Next, leveraging the precision guidance of catalytic nanomotors with *E*-fields, we designed and assembled a chemically powered rotary NEMS by integrating catalytic nanomotors with electric manipulation. First, a rotary NEMS is assembled by *E*-fields following previous reports as illustrated in Figure 5a.[22,77] It consists of a multisegmented Au/Ni nanorod (250 nm in diameter and 8 μm in length) and a patterned nanomagnet (500 nm in diameter) serving as the rotor and bearing, respectively. Different from previous research, the rotor is designed to consist of three Ni segments embedded in the Au nanorod. The structure is Au(200 nm)/Ni(50 nm)/Au(3.5 μm)/Ni(500 nm)/Au(3.5 nm)/Ni(50 nm)/Au(200 nm) as shown in Figure 5b. The Ni segment in the center of the rotor is used to attach the rotary NEMS on the patterned magnetic bearing. The two Ni segments next to the tips aim to anchor the catalytic nanomotors. The patterned nanomagnet has a trilayer stack of Ti (60 nm)/Ni (80 nm)/Cr (6 nm). By using the electric tweezers, the nanorotor is transported and attached atop of the pattern magnetic bearing, where the magnetic interaction between the Ni segment in the rotor and Ni layer in the magnetic bearing fixes the position of the rotary NEMS while still allows its rotation.[22,77] Next, we fabricated catalytic nanomotors made of Pt-AgAu nanowires. Here, we replaced the Au segments used above with Ag(~80 wt %)/Au(~20 wt %) alloy segments in the Pt-based catalytic nanomotors (Figure 5c,d), which can substantially increase the output power and speed. The increase of the speed can be attributed to the much greater potential differences of Pt vs AgAu alloy compared to that of Pt vs pure Au as reported.[37,72] The catalytic nanomotors move at a speed up to ~30 μm/sec in 5 wt % H_2O_2 solution. From the speed, we can estimate the driving force as high as 0.26 piconewtons (pN). With the guidance of the AC *E*-field, the catalytic nanomotor can be efficiently maneuvered toward the rotary NEMS and then be assembled at one end of the rotor by magnetic attraction as shown in Figure 5(e) and movie S5. The assembling process was carried out in 1 wt % H_2O_2 solution to ensure we have sufficient responding time to control and assemble. After assembling, we increased the concentration of H_2O_2 solution to 5 wt %. The nanomotor instantly propelled the NEMS into continuous rotation as shown in Figure 5f and movie S6. The driving torque of the nanomotors in Figure 5f can be readily determined as $1.04 \times 10^{-18} N{\cdot}m$, which is

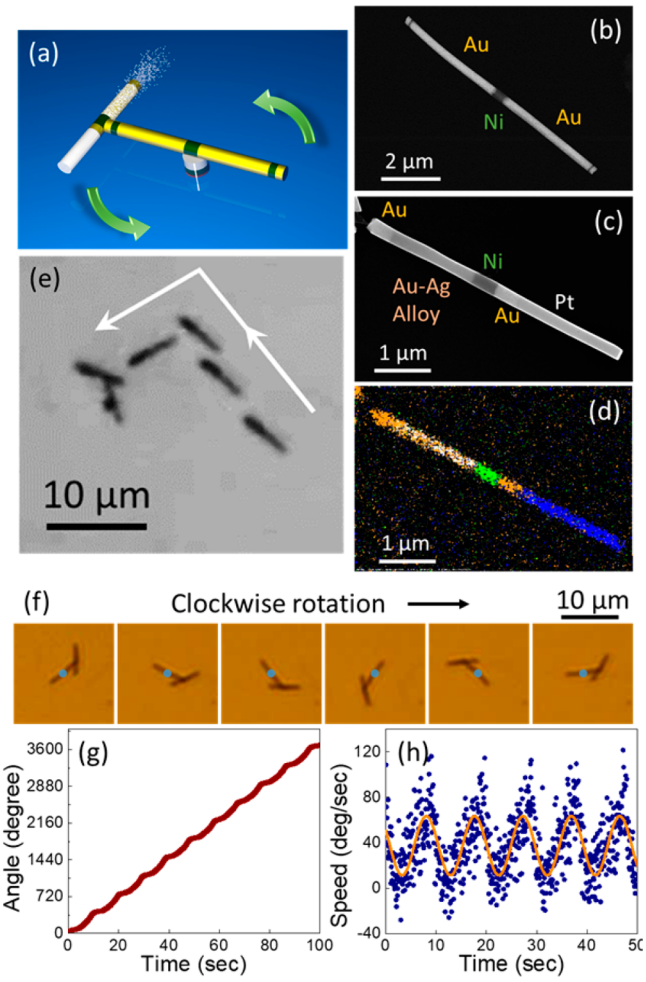

Figure 5. Assembling of catalytic a nanomotor for powering NEMS device into continuous rotation. (a) Schematic diagram of the rotary NEMS device with catalytic nanomotor assembled as the powering component. (b) SEM images of the multisegment nanowire rotor. The segments from left to right are 200 nm Au, 50 nm Ni, 3.5 μm Au, 500 nm Ni, 3.5 μm Au, 50 nm Ni, and 200 nm Au. (c, d) SEM and EDX images of the Pt–Ag/Au catalytic nanomotor. The segments from left to right are 400 nm Au, 1.7 μm Ag–Au alloy, 500 nm Ni, 400 nm Au, and 2 μm Pt. (e) Overlapped snapshots (from movie 5) showing the assembling process of a catalytic nanomotor on a rotary NEMS device. (f) Snapshots (from movie 6) of a rotating NEMS device driven by a catalytic nanomotor taken every 2 s. (g) Rotation angle *versus* time. (h) Rotation speed *versus* time.

sufficient to overcome the friction and magnetic torques between the rotor and bearing as shown in Figure 5(g-h) and movie S6. Here, we can observe the effects of the angle-dependent magnetic force and torque that result in the oscillation of rotation speeds of the rotor with a 360° periodicity as a function of the angular position, agreeing with previous works.[78] The average rotation speed of the NEMS device is determined as 0.64 rad/s.

The approach of integrating powering components to drive nanomechanical devices demonstrated in this work could be applied to assemble various functional components of nanorobots and complicated NEMS/MEMS devices with far-reaching impact in electronics and biomedical research.

DOI: 10.1021/acsnano.7b06824
ACS Nano 2018, 12, 1179–1187

CONCLUSIONS

In summary, we report a highly versatile and precision approach to guide and modulate the propulsions of catalytic nanomotors with *E*-fields, which allows motion control in 2-D and 3-D. The fundamental interactions involved in the electric manipulation have been investigated. Leveraging the precision of manipulation, we experimentally confirmed the inverse linear dependence of speed and size of catalytic nanomotors, supporting previous modeling. For applications, the manipulation strategy provides facile operations of these catalytic nanomotors to realize cargo capture, transport, and delivery to designated microdock. The prowess of the manipulation is also demonstrated by assembling catalytic motors as powering component of rotary NEMS. This work could be inspiring for constructing various nanorobots and functional NEMS/MEMS devices for diverse tasks in electronics and biomedical research.

METHODS

Fabrication of Nanorod Catalytic Nanomotors. Arrays of nanorod catalytic nanomotors were fabricated by electrodeposition into nanoporous templates (Alumina membrane with 250 nm-diamtered pores: Anodisc 47, Catalog No. 6809−5012, Whatman, Germany; polycarbonate membrane with 150 nm-diamtered pores: Nuclepore Track-Etch Membrane, MFG Part No. 110605, Whatman, England) in a three-electrode setup. The three-electrode system consists of a Cu layer on the back of nanoporous template as the working electrode, Pt mesh as the counter electrode, and Ag/AgCl (3 M NaCl) electrode as the reference electrode. The Au electrolyte (434 HS RTU) and Ag electrolyte (white silver solution RTU) are purchased from Technic Inc., Cranston, RI, and used as received. The Pt plating electrolyte, made of 0.017 M $(NH_4)_2PtCl_6$ and 0.25 M Na_2HPO_4, is prepared in the lab. The Ni plating electrolyte, made of 0.08 M $NiCl_2{\cdot}6H_2O$, 1.6 M $Ni(H_2NSO_3)_2$, and 0.32 M H_3BO_3, is prepared in the lab. The deposition of materials was initiated from the Cu film at the bottom of nanopores, the size of which determines the diameter of the nanorods. The amount of electric charges passing through the circuit controls the length of each segment of the nanorods. As a result, arrays of nanorod catalytic nanomotors can be readily synthesized. After centrifuging and dispersing in DI water and ethanol alternatively for at least two times, they were suspended in DI water.

Setup of 3D Electric Manipulation. The setup includes in-plane quadruple microelectrodes patterned on a glass slide and a pair of indium tin oxide (ITO) parallel electrodes assembled in the vertical direction. The bottom ITO electrode is fabricated on the opposite side of the quadruple microelectrodes on the glass (1 mm in thickness). A suspension reservoir is formed on top of the quadruple microelectrodes by a piece of polydimethylsiloxane (PDMS) elastomer (~1 mm in thickness) with a well of ~4 mm in diameter. The top of the well is sealed with a second ITO electrode for providing *E*-field in the vertical direction.

ASSOCIATED CONTENT

Supporting Information

The Supporting Information is available free of charge on the ACS Publications website at DOI: 10.1021/acsnano.7b06824.

Experimental details, velocity analysis, torque calculation, and additional zeta potential and SEM characterization of catalytic nanomotors (PDF)

Random movements of catalytic nanomotor *versus* directional motions of *E*-field guided catalytic nanomotor (2× frame rate) (AVI)

Motions of catalytic nanomotors in the vertical direction with the vertical alignment of the AC *E*-fields. Video on the left: nanomotors stopped with vertical alignment; video on the right: nanomotors move along the vertical direction and finally disappear from the view. Here the concentrations of fuels are 7.5 wt % and 12.5% H_2O_2, respectively (AVI)

Speed modulation of a catalytic nanomotor (2× frame rate) (AVI)

Targeted cargo delivery by a catalytic nanomotor (5× frame rate) (AVI)

Assembling process of a catalytic nanomotor on a rotary NEMS device. The rotary NEMS is driven into rotation (movie was edited and enhanced by Adobe Premiere Pro CC) (AVI)

Rotation of a rotary NEMS device powered by a catalytic nanomotor (5× frame rate) (AVI)

AUTHOR INFORMATION

Corresponding Author

*E-mail: dfan@austin.utexas.edu.

ORCID

Donglei Fan: 0000-0002-4724-2483

Notes

The authors declare no competing financial interest.

ACKNOWLEDGMENTS

This research is supported by the Welch Foundation (F-1734) and National Science Foundation (CMMI 1150767 and EECS 1710922). We thank the inspiring suggestion of size-dependent tests from Professor T. Mallouk (Pennsylvania State University). We also thank Professor P. Fischer (Max Planck Institute, Germany) for the helpful discussion.

REFERENCES

(1) Wang, H.; Pumera, M. Fabrication of Micro/Nanoscale Motors. *Chem. Rev.* **2015**, *115*, 8704−8735.

(2) Guix, M.; Mayorga-Martinez, C. C.; Merkoçi, A. Nano/Micromotors in (Bio)chemical Science Applications. *Chem. Rev.* **2014**, *114*, 6285−6322.

(3) Kim, K.; Guo, J.; Xu, X.; Fan, D. L. Recent Progress on Man-Made Inorganic Nanomachines. *Small* **2015**, *11*, 4037−4057.

(4) Kim, K.; Guo, J.; Liang, Z. X.; Zhu, F. Q.; Fan, D. L. Man-Made Rotary Nanomotors: A Review Of Recent Developments. *Nanoscale* **2016**, *8*, 10471−10490.

(5) Wang, J.; Gao, W. Nano/Microscale Motors: Biomedical Opportunities and Challenges. *ACS Nano* **2012**, *6*, 5745−5751.

(6) Xu, T.; Gao, W.; Xu, L. P.; Zhang, X.; Wang, S. Fuel-Free Synthetic Micro-/Nanomachines. *Adv. Mater.* **2017**, *29*, 1603250.

(7) Wang, W.; Li, S.; Mair, L.; Ahmed, S.; Huang, T. J.; Mallouk, T. E. Acoustic Propulsion of Nanorod Motors Inside Living Cells. *Angew. Chem.* **2014**, *126*, 3265−3268.

(8) Qiu, T.; Lee, T. C.; Mark, A. G.; Morozov, K. I.; Münster, R.; Mierka, O.; Turek, S.; Leshansky, A. M.; Fischer, P. Swimming by Reciprocal Motion at Low Reynolds Number. *Nat. Commun.* **2014**, *5*, 5119.

(9) Palagi, S.; Mark, A. G.; Reigh, S. Y.; Melde, K.; Qiu, T.; Zeng, H.; Parmeggiani, C.; Martella, D.; Sanchez-Castillo, A.; Kapernaum, N.; Giesselmann, F.; Wiersma, D. S.; Lauga, E.; Fischer, P. Structured Light Enables Biomimetic Swimming and Versatile Locomotion of Photoresponsive Soft Microrobots. *Nat. Mater.* **2016**, *15*, 647−653.

(10) Kim, K.; Guo, J.; Liang, Z.; Fan, D. Artificial Micro/Nanomachines for Bio-applications: Biochemical Delivery and Diagnostic Sensing. *Adv. Funct. Mater.* **2018**, DOI: 10.1002/adfm.201705867.

(11) Soong, R. K.; Bachand, G. D.; Neves, H. P.; Olkhovets, A. G.; Craighead, H. G.; Montemagno, C. D. Powering an Inorganic

DOI: 10.1021/acsnano.7b06824
ACS Nano 2018, 12, 1179−1187

Nanodevice with a Biomolecular Motor. *Science* **2000**, *290*, 1555−1558.
(12) Fennimore, A. M.; Yuzvinsky, T. D.; Han, W. Q.; Fuhrer, M. S.; Cumings, J.; Zettl, A. Rotational Actuators Based on Carbon Nanotubes. *Nature* **2003**, *424*, 408.
(13) Paxton, W. F.; Kistler, K. C.; Olmeda, C. C.; Sen, A.; St. Angelo, S. K.; Cao, Y.; Mallouk, T. E.; Lammert, P. E.; Crespi, V. H. Catalytic Nanomotors: Autonomous Movement of Striped Nanorods. *J. Am. Chem. Soc.* **2004**, *126*, 13424−13431.
(14) Fournier-Bidoz, S.; Arsenault, A. C.; Manners, I.; Ozin, G. A. Synthetic Self-Propelled Nanorotors. *Chem. Commun.* **2005**, 441−443.
(15) Liu, M.; Zentgraf, T.; Liu, Y.; Bartal, G.; Zhang, X. Light-Driven Nanoscale Plasmonic Motors. *Nat. Nanotechnol.* **2010**, *5*, 570.
(16) Chiou, P. Y.; Ohta, A. T.; Wu, M. C. Massively Parallel Manipulation of Single Cells and Microparticles Using Optical Images. *Nature* **2005**, *436*, 370.
(17) Ghosh, A.; Fischer, P. Controlled Propulsion of Artificial Magnetic Nanostructured Propellers. *Nano Lett.* **2009**, *9*, 2243−2245.
(18) Gao, W.; Sattayasamitsathit, S.; Manesh, K. M.; Weihs, D.; Wang, J. Magnetically Powered Flexible Metal Nanowire Motors. *J. Am. Chem. Soc.* **2010**, *132*, 14403−14405.
(19) Zhang, L.; Petit, T.; Lu, Y.; Kratochvil, B. E.; Peyer, K. E.; Pei, R.; Lou, J.; Nelson, B. J. Controlled Propulsion and Cargo Transport of Rotating Nickel Nanowires near a Patterned Solid Surface. *ACS Nano* **2010**, *4*, 6228−6234.
(20) Medina-Sánchez, M.; Schwarz, L.; Meyer, A. K.; Hebenstreit, F.; Schmidt, O. G. Cellular Cargo Delivery: Toward Assisted Fertilization by Sperm-Carrying Micromotors. *Nano Lett.* **2016**, *16*, 555−561.
(21) Han, K.; Shields, C. W.; Diwakar, N. M.; Bharti, B.; López, G. P.; Velev, O. D. Sequence-Encoded Colloidal Origami and Microbot Assemblies from Patchy Magnetic Cubes. *Sci. Adv.* **2017**, *3*, e1701108.
(22) Kim, K.; Xu, X.; Guo, J.; Fan, D. L. Ultrahigh-Speed Rotating Nanoelectromechanical System Devices Assembled from Nanoscale Building Blocks. *Nat. Commun.* **2014**, *5*, 3632.
(23) Fan, D.; Yin, Z.; Cheong, R.; Zhu, F. Q.; Cammarata, R. C.; Chien, C. L.; Levchenko, A. Subcellular-Resolution Delivery of A Cytokine Through Precisely Manipulated Nanowires. *Nat. Nanotechnol.* **2010**, *5*, 545.
(24) Xu, X.; Kim, K.; Fan, D. Tunable Release of Multiplex Biochemicals by Plasmonically Active Rotary Nanomotors. *Angew. Chem., Int. Ed.* **2015**, *54*, 2525−2529.
(25) Chang, S. T.; Paunov, V. N.; Petsev, D. N.; Velev, O. D. Remotely Powered Self-Propelling Particles and Micropumps Based on Miniature Diodes. *Nat. Mater.* **2007**, *6*, 235.
(26) Wang, W.; Castro, L. A.; Hoyos, M.; Mallouk, T. E. Autonomous Motion of Metallic Microrods Propelled by Ultrasound. *ACS Nano* **2012**, *6*, 6122−6132.
(27) Garcia-Gradilla, V.; Orozco, J.; Sattayasamitsathit, S.; Soto, F.; Kuralay, F.; Pourazary, A.; Katzenberg, A.; Gao, W.; Shen, Y.; Wang, J. Functionalized Ultrasound-Propelled Magnetically Guided Nanomotors: Toward Practical Biomedical Applications. *ACS Nano* **2013**, *7*, 9232−9240.
(28) Ding, X.; Lin, S. S.; Kiraly, B.; Yue, H.; Li, S.; Chiang, I.; Kao; Shi, J.; Benkovic, S. J.; Huang, T. J. On-Chip Manipulation of Single Microparticles, Cells, and Organisms Using Surface Acoustic Waves. *Proc. Natl. Acad. Sci. U. S. A.* **2012**, *109*, 11105−11109.
(29) Li, J.; Esteban-Fernández de Ávila, B.; Gao, W.; Zhang, L.; Wang, J. Micro/nanorobots for Biomedicine: Delivery, Surgery, Sensing, and Detoxification. *Sci. Robot.* **2017**, *2*, eaam6431.
(30) Wang, W.; Duan, W.; Ahmed, S.; Mallouk, T. E.; Sen, A. Small Power: Autonomous Nano- and Micromotors Propelled by Self-generated Gradients. *Nano Today* **2013**, *8*, 531−554.
(31) Ma, X.; Hortelão, A. C.; Patiño, T.; Sánchez, S. Enzyme Catalysis To Power Micro/Nanomachines. *ACS Nano* **2016**, *10*, 9111−9122.
(32) Wong, F.; Sen, A. Progress toward Light-Harvesting Self-Electrophoretic Motors: Highly Efficient Bimetallic Nanomotors and Micropumps in Halogen Media. *ACS Nano* **2016**, *10*, 7172−7179.
(33) Wang, W.; Chiang, T.-Y.; Velegol, D.; Mallouk, T. E. Understanding the Efficiency of Autonomous Nano- and Microscale Motors. *J. Am. Chem. Soc.* **2013**, *135*, 10557−10565.
(34) Lin, X.; Wu, Z.; Wu, Y.; Xuan, M.; He, Q. Self-Propelled Micro-/Nanomotors Based on Controlled Assembled Architectures. *Adv. Mater.* **2016**, *28*, 1060−1072.
(35) Mirkovic, T.; Zacharia, N. S.; Scholes, G. D.; Ozin, G. A. Fuel for Thought: Chemically Powered Nanomotors Out-Swim Nature's Flagellated Bacteria. *ACS Nano* **2010**, *4*, 1782−1789.
(36) Wang, H.; Zhao, G.; Pumera, M. Beyond Platinum: Bubble-Propelled Micromotors Based on Ag and MnO2 Catalysts. *J. Am. Chem. Soc.* **2014**, *136*, 2719−2722.
(37) Demirok, U. K.; Laocharoensuk, R.; Manesh, K. M.; Wang, J. Ultrafast Catalytic Alloy Nanomotors. *Angew. Chem., Int. Ed.* **2008**, *47*, 9349−9351.
(38) Laocharoensuk, R.; Burdick, J.; Wang, J. Carbon-Nanotube-Induced Acceleration of Catalytic Nanomotors. *ACS Nano* **2008**, *2*, 1069−1075.
(39) Solovev, A. A.; Mei, Y.; Bermúdez Ureña, E.; Huang, G.; Schmidt, O. G. Catalytic Microtubular Jet Engines Self-Propelled by Accumulated Gas Bubbles. *Small* **2009**, *5*, 1688−1692.
(40) Solovev, A. A.; Xi, W.; Gracias, D. H.; Harazim, S. M.; Deneke, C.; Sanchez, S.; Schmidt, O. G. Self-Propelled Nanotools. *ACS Nano* **2012**, *6*, 1751−1756.
(41) Li, J.; Liu, W.; Wang, J.; Rozen, I.; He, S.; Chen, C.; Kim, H. G.; Lee, H.; Lee, H.; Kwon, S.; Li, T.; Li, L.; Wang, J.; Mei, Y. Nanoconfined Atomic Layer Deposition of TiO2/Pt Nanotubes: Toward Ultrasmall Highly Efficient Catalytic Nanorockets. *Adv. Funct. Mater.* **2017**, *27*, 1700598.
(42) Baraban, L.; Makarov, D.; Streubel, R.; Mönch, I.; Grimm, D.; Sanchez, S.; Schmidt, O. G. Catalytic Janus Motors on Microfluidic Chip: Deterministic Motion for Targeted Cargo Delivery. *ACS Nano* **2012**, *6*, 3383−3389.
(43) Manjare, M.; Yang, B.; Zhao, Y. P. Bubble Driven Quasioscillatory Translational Motion of Catalytic Micromotors. *Phys. Rev. Lett.* **2012**, *109*, 128305.
(44) Dong, R.; Zhang, Q.; Gao, W.; Pei, A.; Ren, B. Highly Efficient Light-Driven TiO2−Au Janus Micromotors. *ACS Nano* **2016**, *10*, 839−844.
(45) Yoshizumi, Y.; Honegger, T.; Berton, K.; Suzuki, H.; Peyrade, D. Trajectory Control of Self-Propelled Micromotors Using AC Electrokinetics. *Small* **2015**, *11*, 5630−5635.
(46) Gao, W.; Pei, A.; Dong, R.; Wang, J. Catalytic Iridium-Based Janus Micromotors Powered by Ultralow Levels of Chemical Fuels. *J. Am. Chem. Soc.* **2014**, *136*, 2276−2279.
(47) Ma, X.; Wang, X.; Hahn, K.; Sánchez, S. Motion Control of Urea-Powered Biocompatible Hollow Microcapsules. *ACS Nano* **2016**, *10*, 3597−3605.
(48) Dey, K. K.; Zhao, X.; Tansi, B. M.; Méndez-Ortiz, W. J.; Córdova-Figueroa, U. M.; Golestanian, R.; Sen, A. Micromotors Powered by Enzyme Catalysis. *Nano Lett.* **2015**, *15*, 8311−8315.
(49) Jang, B.; Hong, A.; Kang, H. E.; Alcantara, C.; Charreyron, S.; Mushtaq, F.; Pellicer, E.; Büchel, R.; Sort, J.; Lee, S. S.; Nelson, B. J.; Pané, S. Multiwavelength Light-Responsive Au/B-TiO2 Janus Micromotors. *ACS Nano* **2017**, *11*, 6146−6154.
(50) Burdick, J.; Laocharoensuk, R.; Wheat, P. M.; Posner, J. D.; Wang, J. Synthetic Nanomotors in Microchannel Networks: Directional Microchip Motion and Controlled Manipulation of Cargo. *J. Am. Chem. Soc.* **2008**, *130*, 8164.
(51) Peng, F.; Tu, Y.; van Hest, J. C. M.; Wilson, D. A. Self-Guided Supramolecular Cargo-Loaded Nanomotors with Chemotactic Behavior towards Cells. *Angew. Chem., Int. Ed.* **2015**, *54*, 11662−11665.
(52) Mou, F.; Chen, C.; Zhong, Q.; Yin, Y.; Ma, H.; Guan, J. Autonomous Motion and Temperature-Controlled Drug Delivery of Mg/Pt-Poly(N-isopropylacrylamide) Janus Micromotors Driven by Simulated Body Fluid and Blood Plasma. *ACS Appl. Mater. Interfaces* **2014**, *6*, 9897−9903.

DOI: 10.1021/acsnano.7b06824
ACS Nano 2018, 12, 1179−1187

(53) Li, J.; Shklyaev, O. E.; Li, T.; Liu, W.; Shum, H.; Rozen, I.; Balazs, A. C.; Wang, J. Self-Propelled Nanomotors Autonomously Seek and Repair Cracks. *Nano Lett.* **2015**, *15*, 7077−7085.
(54) Li, J.; Gao, W.; Dong, R.; Pei, A.; Sattayasamitsathit, S.; Wang, J. Nanomotor Lithography. *Nat. Commun.* **2014**, *5*, 5026.
(55) Gao, W.; Dong, R.; Thamphiwatana, S.; Li, J.; Gao, W.; Zhang, L.; Wang, J. Artificial Micromotors in the Mouse's Stomach: A Step toward *in vivo* Use of Synthetic Motors. *ACS Nano* **2015**, *9*, 117−123.
(56) Xu, T.; Soto, F.; Gao, W.; Dong, R.; Garcia-Gradilla, V.; Magana, E.; Zhang, X.; Wang, J. Reversible Swarming and Separation of Self-Propelled Chemically Powered Nanomotors under Acoustic Fields. *J. Am. Chem. Soc.* **2015**, *137*, 2163−2166.
(57) Balasubramanian, S.; Kagan, D.; Manesh, K. M.; Calvo-Marzal, P.; Flechsig, G.-U.; Wang, J. Thermal Modulation of Nanomotor Movement. *Small* **2009**, *5*, 1569−1574.
(58) Solovev, A. A.; Smith, E. J.; Bufon, C. C. B.; Sanchez, S.; Schmidt, O. G. Light-Controlled Propulsion of Catalytic Microengines. *Angew. Chem., Int. Ed.* **2011**, *50*, 10875−10878.
(59) Ibele, M.; Mallouk, T. E.; Sen, A. Schooling Behavior of Light-Powered Autonomous Micromotors in Water. *Angew. Chem., Int. Ed.* **2009**, *48*, 3308−3312.
(60) Moo, J. G. S.; Presolski, S.; Pumera, M. Photochromic Spatiotemporal Control of Bubble-Propelled Micromotors by a Spiropyran Molecular Switch. *ACS Nano* **2016**, *10*, 3543−3552.
(61) Calvo-Marzal, P.; Manesh, K. M.; Kagan, D.; Balasubramanian, S.; Cardona, M.; Flechsig, G.-U.; Posner, J.; Wang, J. Electrochemically-Triggered Motion of Catalytic Nanomotors. *Chem. Commun.* **2009**, 4509−4511.
(62) Wang, W.; Duan, W.; Zhang, Z.; Sun, M.; Sen, A.; Mallouk, T. E. A Tale of Two Forces: Simultaneous Chemical and Acoustic Propulsion of Bimetallic Micromotors. *Chem. Commun.* **2015**, *51*, 1020−1023.
(63) Chien, C. L.; Fan, D.; Cammarata, R. C. System and Method for Precision Transport, Positioning, and Assembling of Longitudinal Nano-structures. Patent US 9,044,808 B2, 2015.
(64) Whitney, T. M.; Jiang, J. S.; Searson, P. C.; Chien, C. L. Fabrication And Magnetic Properties of Arrays of Metallic Nanowires. *Science* **1993**, *261*, 1316−1319.
(65) Jones, T. B. *Electromechanics of Particles*; Cambridge University Press: New York, 2005.
(66) *Hydrogen Peroxide Physical Properties Data Book*; Becco Chemical Division, 1955.
(67) Paxton, W. F.; Baker, P. T.; Kline, T. R.; Wang, Y.; Mallouk, T. E.; Sen, A. Catalytically Induced Electrokinetics for Motors and Micropumps. *J. Am. Chem. Soc.* **2006**, *128*, 14881−14888.
(68) Paxton, W. F.; Sen, A.; Mallouk, T. E. Motility of Catalytic Nanoparticles through Self-Generated Forces. *Chem. - Eur. J.* **2005**, *11*, 6462−6470.
(69) Liu, R.; Sen, A. Autonomous Nanomotor Based on Copper−Platinum Segmented Nanobattery. *J. Am. Chem. Soc.* **2011**, *133*, 20064−20067.
(70) Wang, H.; Moo, J. G. S.; Pumera, M. From Nanomotors to Micromotors: The Influence of the Size of an Autonomous Bubble-Propelled Device upon Its Motion. *ACS Nano* **2016**, *10*, 5041−5050.
(71) Lee, T.-C.; Alarcón-Correa, M.; Miksch, C.; Hahn, K.; Gibbs, J. G.; Fischer, P. Self-Propelling Nanomotors in the Presence of Strong Brownian Forces. *Nano Lett.* **2014**, *14*, 2407−2412.
(72) Kagan, D.; Calvo-Marzal, P.; Balasubramanian, S.; Sattayasamitsathit, S.; Manesh, K. M.; Flechsig, G.-U.; Wang, J. Chemical Sensing Based on Catalytic Nanomotors: Motion-Based Detection of Trace Silver. *J. Am. Chem. Soc.* **2009**, *131*, 12082−12083.
(73) Baker, D. R. *Capillary Electrophoresis*; John Wiley & Sons, Inc., 1995.
(74) Barz, D. P. J.; Vogel, M. J.; Steen, P. H. Determination of the Zeta Potential of Porous Substrates by Droplet Deflection. I. The Influence of Ionic Strength and pH Value of an Aqueous Electrolyte in Contact with a Borosilicate Surface. *Langmuir* **2009**, *25*, 1842−1850.
(75) Kline, T. R.; Paxton, W. F.; Wang, Y.; Velegol, D.; Mallouk, T. E.; Sen, A. Catalytic Micropumps: Microscopic Convective Fluid Flow and Pattern Formation. *J. Am. Chem. Soc.* **2005**, *127*, 17150−17151.
(76) Esplandiu, M. J.; Afshar Farniya, A.; Bachtold, A. Silicon-Based Chemical Motors: An Efficient Pump for Triggering and Guiding Fluid Motion Using Visible Light. *ACS Nano* **2015**, *9*, 11234−11240.
(77) Guo, J.; Kim, K.; Lei, K. W.; Fan, D. L. Ultra-Durable Rotary Micromotors Assembled from Nanoentities by Electric Fields. *Nanoscale* **2015**, *7*, 11363−11370.
(78) Kim, K.; Guo, J.; Xu, X.; Fan, D. Micromotors with Step-Motor Characteristics by Controlled Magnetic Interactions among Assembled Components. *ACS Nano* **2015**, *9*, 548−554.

DOI: 10.1021/acsnano.7b06824
ACS Nano 2018, 12, 1179−1187